NANO LETTERS

2001
Vol. 1, No. 12
743−748

Controlled Synthesis of Semiconductor PbS Nanocrystals and Nanowires Inside Mesoporous Silica SBA-15 Phase

Feng Gao,[†] Qingyi Lu,[†] Xiaoying Liu,[†] Yushan Yan,[‡] and Dongyuan Zhao*,[†]

Department of Chemistry, Fudan University, Shanghai 200433, P. R. China, and Department of Chemical and Environmental Engineering, University of California, Riverside, California 92521

Received September 29, 2001; *Revised Manuscript Received October 10, 2001*

ABSTRACT

A new flexible approach is developed to fabricate uniform nanocrystals and nanowires of binary compound semiconductor PbS inside the channels of mesoporous silica SBA-15. The approach combines functionalization of the channel surface with thiol groups, absorption of Pb^{2+}, and heating in N_2 atmosphere at high temperature. The separate introduction of thiol groups and Pb^{2+} makes the loading of a binary compound efficient and as easy as the loading of a single element. The nanocrystals are uniform and their sizes (5 nm) are consistent with the diameter of mesoporous SBA-15. The diameter of the PbS nanowires is about 6 nm and the length is several hundred nanometers. TEM images first intuitively confirm the formation of binary sulfide nanocrystals and nanowires dispersing uniformly inside the channels of mesoporous SBA-15. The key for transition from nanocrystals to nanowires is to increase the amount of the Si–OH group on the channel surface of SBA-15, and ethanol extraction proves to be effective to keep large amount of Si–OH groups during removing of the block copolymer. A massive blue shift is observed in photoluminescence spectra, and this clearly shows the quantum size effects of the PbS nanocrystals and nanowires.

Compound II−VI semiconductor nanocrystals and nanowires have unique electronic and optical properties and are useful in novel nanodevices such as light-emitting diodes,[1] single-electron transistors,[2] and field-effect thin-film transistors.[3] The properties of semiconductor nanocrystals and nanowires are highly size-dependent,[4] and thus precise control of their size and size distribution is of critical importance. As one of the II−VI semiconductors, PbS in its bulk form has a near-infrared band gap of 0.41 eV. Its band gap can be widened to the visible region of about 2 eV by forming nanoclusters.[5] Consequently, PbS nanocrystals and nanowires are potentially useful in electroluminescent devices such as light-emitting diodes. Quantum-sized PbS also has exceptional third-order nonlinear optical properties,[6] making it be useful in optical devices such as optical switches. PbS nanocrystals and nanowires have been prepared in polymers,[7,8] in zeolites,[9] in block copolymer nanoreactors,[10] and in reverse liquid crystals through γ-radiation.[11] However, most of these fabrication techniques result in nanowires with diameter too large to exhibit quantum confinement effects. Mesoporous silica MCM-41 with regular array of cylindrical channels[12] has been used for confined growth of semiconductor quantum dots and quantum wires.[13−22] Nanocrystals of the II−VI group semiconductor that have been synthesized inside MCM-41 silica so far include CdSe,[13] ZnO,[14] and ZnS.[15] However, in all cases the nanocrystals may be located randomly inside or even outside of the mesoporous channels because their presence was only confirmed by XRD or optical spectra and no direct proof from TEM images was given. Recently, mesoporous silica SBA-15 with larger channels and higher thermal and hydrothermal stability than MCM-41 was synthesized by using triblock copolymer as the template.[23] SBA-15 has been explored for synthesis of noble metal Ag, Au, Pt, Ph, and Si nanowires.[24−27] However, synthesis of binary compound semiconductor nanocrystals and nanowires inside SBA-15 has not been reported.

In this paper, we report a new flexible fabrication technique that can produce both PbS nanocrystals and nanowires with uniform size. Binary compound semiconductor PbS nanowires with uniform diameter (6 nm) have not been reported by any other methods. This approach combines a surface modification scheme with a wet impregnation technique to confine PbS nanocrystals and nanowires inside the channels of SBA-15. The transition from nanocrystals to nanowires was made possible by increasing the loading of the inorganic compound in the meso-channels through increasing the number density of the Si−OH and subsequently −SH functional groups. Specifically, the triblock copolymer template was removed from the as-synthesized SBA-15 either by calcinations to form Cal-SBA-15 for nanocrystal synthesis or by extraction with ethanol to obtain

* Corresponding author: E-mail: dyzhao@fudan.edu.cn.
[†] Fudan University.
[‡] University of California.

10.1021/nl0156383 CCC: $20.00
Published on Web 10/20/2001

Scheme 1

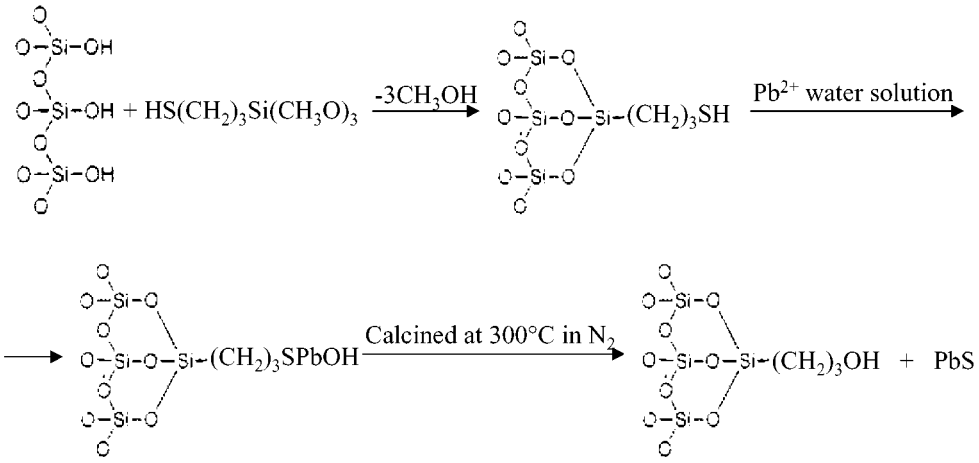

Ext-SBA-15 for nanowire synthesis. The ethanol extraction method leaves behind more Si−OH groups than does high-temperature calcination. The template-free SBA-15 was functionalized with thiol groups to obtain SH-Cal-SBA-15 and SH-Ext-SBA-15. Finally, Pb^{2+} was introduced into SH-SBA-15, followed by heating at high temperature in N_2 atmosphere to form the final PbS-particle-SBA-15 and PbS-wire-SBA-15 (Scheme 1). The technique presented here is advantageous in that it introduces −S and Pb^{2+} in two separate steps under a nonreactive environment, leading to efficient loading of both −SH and Pb^{2+}. Clearly the loading of binary compound here has been made as easy as loading a single element.

Template-containing mesoporous silica SBA-15 was synthesized according to a published procedure using Pluronic P123 ($EO_{20}PO_{70}EO_{20}$, M_{av} = 5800, Aldrich) and tetraethyl orthosilicate (TEOS, 98%, Aldrich) under acid conditions.[23] In a typical synthesis, 2 g of P123 was dissolved under stirring into 15 g of distilled water and 60 g of 2M HCl aqueous solution. Then 4.15 g of TEOS was added into the homogeneous solution. After the mixture was stirred at 35 ∼ 40 °C for 20 h and crystallized at 100 °C for 2 days, the solid product was collected by filtering. The P123 triblock copolymer was either removed by calcination at 550 °C for 6 h to obtain Cal-SBA-15 or by ethanol extraction for 2 days to obtain Ext-SBA-15.

The synthesis procedure of PbS-particle-SBA-15 was as follows. One gram of Cal-SBA-15 was dried in a vacuum oven at 150 °C for at least 2 h. The dried sample was then suspended in 100 mL of 5% v/v solution of (3-thiolpropyl)-trimethoxysilane (SH) in dry toluene for 24 h to obtain SH-Cal-SBA-15. The SH-Cal-SBA-15 sample was collected by filtering, then washed with an ample amount of toluene, and finally dried in a vacuum. To introduce Pb^{2+} into SBA-15, 0.2 g of SH-Cal-SBA-15 was soaked in 20 mL ethanol solution containing 0.379 g of $PbAc_2 \cdot 3H_2O$. After stirring at room temperature for 40 h, the mixture was filtered and washed with ethanol and then distilled water for several times to remove extra Pb^{2+} on the outside of SBA-15. The obtained Pb-SH-Cal-SBA-15 was heated at 300 °C for 2 h in N_2 atmosphere to form PbS-particle-SBA-15. PbS-wire-SBA-15 was similarly obtained by using Ext-SBA-15. Low-angle and wide-angle powder X-ray diffraction (XRD) patterns were obtained on a Rigaku D/Max-IIA using filtered Cu Kα radiation. N_2 adsorption−desorption isotherms were obtained at 77 K using a Micromeritics Tristar 3000 analyzer. The Barrett-Emmett-Tellter (BET) equation was applied for calculation of specific surface area and the Barrett-Joyner-Halanda (BJH) formula for pore volume and pore size distribution by using the desorption branch of the isotherm. For transmission electron microscopy (TEM) measurements, the powder was ground in ethanol and then dispersed on a holey carbon-coated copper grid. TEM was performed in a Philips CM200-FEG at an accelerating voltage of 120 kV with a very low illumination to avoid destruction of the

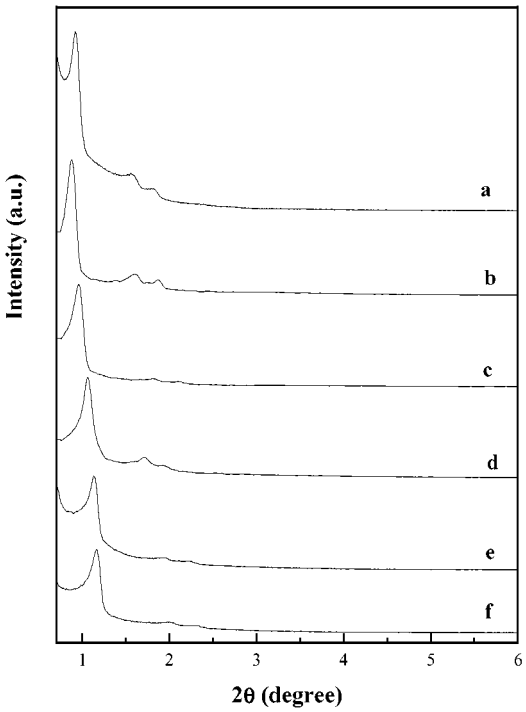

Figure 1. Low-angle XRD patterns of primary mesoporous SBA-15 samples. (a) Cal-SBA-15; (b) Ext-SBA-15; (c) SH-Cal-SBA-15; (d) SH-Ext-SBA-15; (e) PbS-particle-SBA-15; (f) PbS-wire-SBA-15.

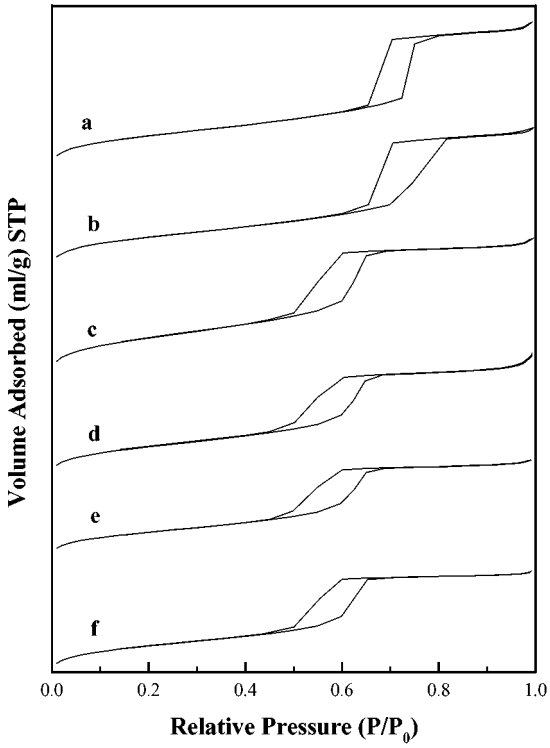

Figure 2. Nitrogen adsorption−desorption isotherms of SBA-15 samples. (a) Cal-SBA-15; (b) Ext-SBA-15; (c) SH-Cal-SBA-15; (d) SH-Ext-SBA-15; (e) PbS-particle-SBA-15; (f) PbS-wire-SBA-15.

Table 1: Parameters of the SBA-15 Samples

sample	d_{100} (Å)	surface area (m^2/g)	pore diam (Å)	pore vol (cm^3/g)
Cal-SBA-15	94.3	680	79	0.977
SH-Cal SBA-15	82.2	587	54	0.724
PbS-particle-SBA-15	75.1	505	51	0.670
Ext-SBA-15	99.9	660	78	1.004
SH-Ext-SBA-15	79.4	434	55	0.601
PbS-wire-SBA-15	74.9	344	48	0.519

material under the electron beam. Energy dispersive spectra (EDS) were obtained using an EDAX DX-4 analytical system. Photoluminescence (PL) spectra were recorded in a Renishow 2000 with an Ar ion laser at room temperature. The excitation wavelength for PbS was 514.5 nm.

Figure 1 shows the low-angle XRD patterns of Cal-SBA-15, Ext-SBA-15, SH-Cal-SBA-15, SH-Ext-SBA-15, PbS-particle-SBA-15, and PbS-wire-SBA-15. All XRD patterns display three reflection peaks that are characteristic of hexagonal mesoporous silica SBA-15. This shows that the primary SBA-15 silica of high quality is obtained after calcination and ethanol extraction (Figures 1a and 1b), and its ordered hexagonal mesostructure is maintained during the functionalization of the channel surface with thiol groups and the formation of PbS nanocrystals and nanowires. The functionalization leads to a decrease in intensity of the peaks (Figure 1c and 1d). The organic component has been shown to decrease the intensity of the XRD peaks,[28] and therefore the observed reduction suggests successful surface modification. The formation of PbS nanocrystals and nanowires leads

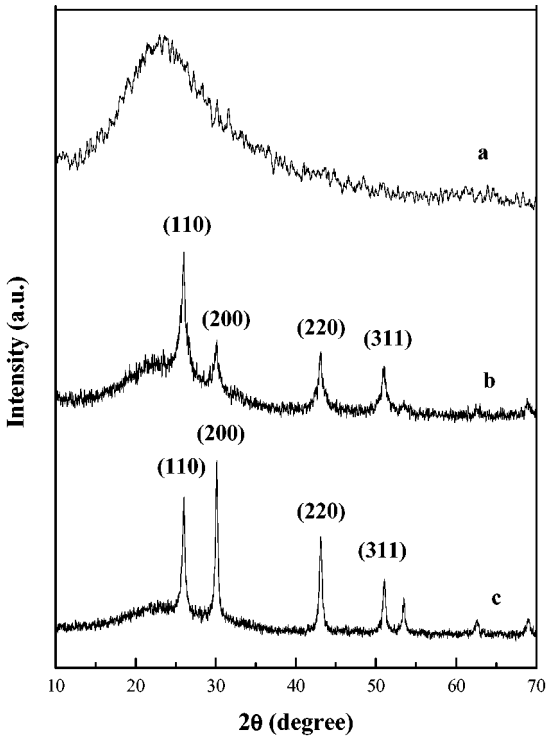

Figure 3. Wide-angle XRD patterns of the SBA-15 samples. (a) Cal-SBA-15; (b) PbS-particle-SBA-15; (c) PbS-wire-SBA-15.

to a further decrease in the intensity of the peaks (Figure 1e and 1f), confirming the pore filling of the host material because pore filling can reduce the scattering contrast between the pores and the walls of the mesoporous material.[29] Additionally, the peaks of SH-SBA-15 and PbS-SBA-15 are slightly shifted to higher angle (Figure 1 and Table 1), and this may be attributed to contraction of framework during the support treatment. Figure 2 shows the nitrogen adsorption−desorption isotherms for SBA-15, SH−SBA-15, and PbS-SBA-15. All of the isotherms are of type IV classification, which is typical of adsorption of mesoporous materials.[30] A well-defined step occurs approximately at $p/p_0 = 0.6\sim0.8$, which is associated with the filling of the mesopores due to capillary condensation. After formation of nanocrystals and nanowires, the amount of adsorbed nitrogen decreases and the inflection point of the step shifts to a smaller p/p_0. The effects can be attributed to the introduction of PbS nanocrystals and nanowires inside the channels of SBA-15. The reduced amount of nitrogen absorption is caused by a smaller specific surface, while the shift of the step to lower relative pressure is indicative of smaller pore sizes. Table 1 summarizes the parameters of the samples calculated from nitrogen sorption studies by applying the BET equation for specific surface area and the BJH formula for pore size distribution.[31,32] Both PbS-particle-SBA-15 and PbS-wire-SBA-15 still show mesoporosity, suggesting that PbS nanocrystals and nanowires are dispersed throughout the channels and the mesoporous channels are still maintained.

Figure 3 shows the wide-angle XRD patterns of the parent SBA-15 and PbS-SBA-15 samples. In Figure 3a, the very broad XRD reflection peak at 26° comes from the diffraction of the amorphous wall of SBA-15. The nanocrystal and

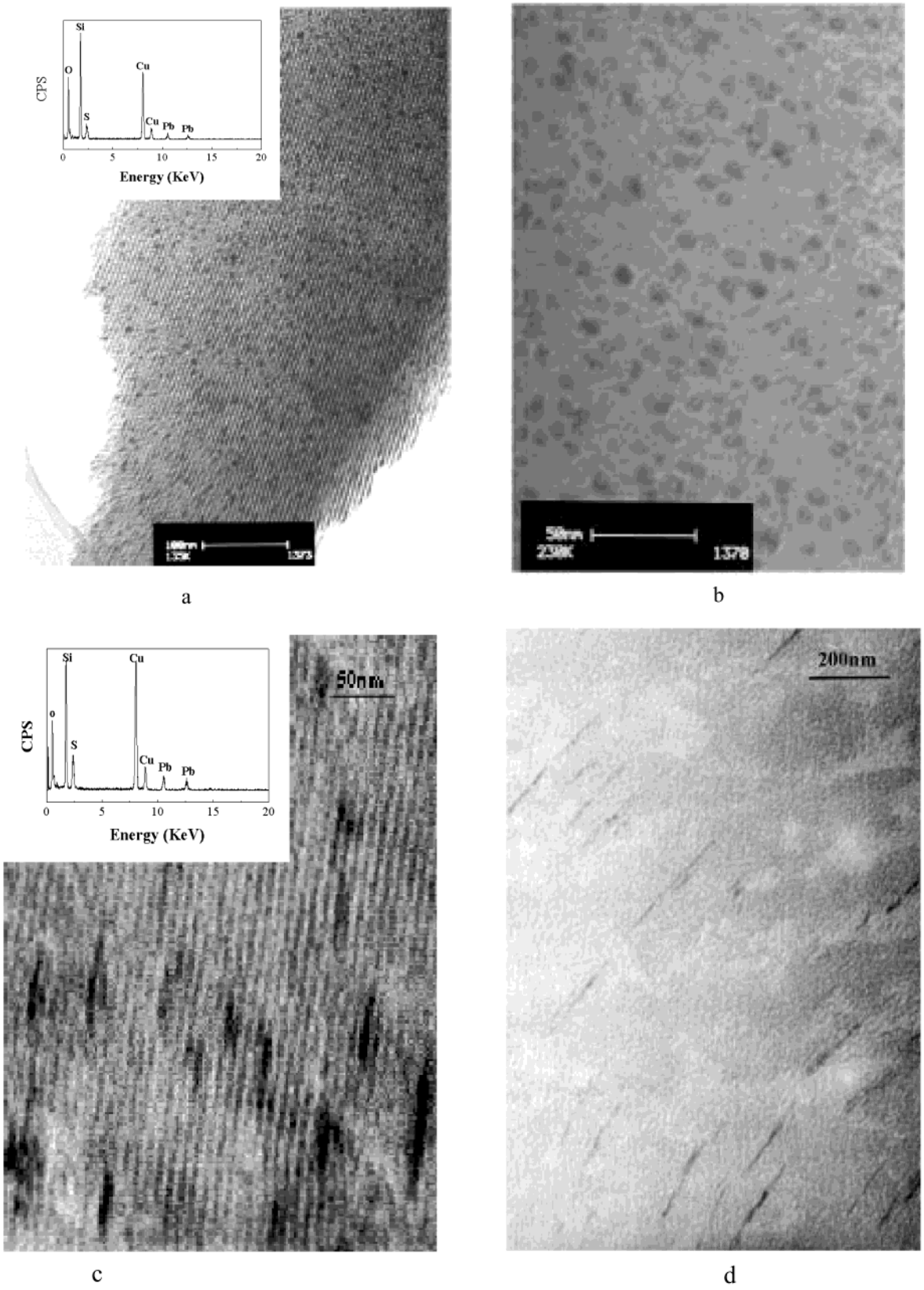

Figure 4. TEM micrographs of PbS−SBA-15 sample: (a) PbS-particle-SBA-15 (inset: EDS spectrum of PbS-particle-SBA-15); (b) PbS nanoparticles obtained by destruction of the parent SBA-15; (c) PbS-wire-SBA-15 (inset: EDS spectrum of PbS-wire-SBA-15); (d) PbS nanowires obtained by destruction of the parent SBA-15.

nanowire loaded SBA-15 silicas (Figure 3b and 3c) show sharp peaks that can be indexed as galena phase PbS with lattice constants comparable to the values of JCPDS card (No. 5-592). The XRD peaks are relatively broad due to the small size of the nanocrystal and nanowires. By using the Scherrer diffraction formula ($d = k\lambda/\beta\cos\theta$), the nanocrystal

size is calculated to be 5 nm for the nanoparticle and 6 nm for the nanowires, consistent with the pore diameter of SH-Cal-SBA-15 and SH-Ext-SBA-15, respectively. This indicates the confinement of PbS nanoparticles and nanowires with the galena crystalline phase inside the meso-channels of SBA-15. It is known that nanosized materials are easy to sinter when they are thermally treated, unless their growth is somehow confined. The nanocrystal and nanowire loaded samples were calcined at 600 °C for 3 h in nitrogen and no changes in XRD patterns were detected (not shown), suggesting that the limited space of SBA-15 restricted the growth of PbS nanocrystals and nanowires.

The PbS nanocrystals and nanowires inside the channels of SBA-15 are further confirmed by TEM (Figure 4). The highly ordered pore structure of SBA-15 is preserved during the formation of binary PbS nanocrystals and nanowires. Figure 4a shows clearly that PbS nanocrystals appear as dark spherical objects between the walls of SBA-15 and are homogeneously distributed inside the channels of SBA-15. By destruction of the SBA-15 framework, PbS nanocrystals with uniform size are obtained (Figure 4b). The average crystal size is about 5 nm, which is consistent with the channel diameter of the parent SH-Cal-SBA-15. An EDS analysis carried out on the mesoporous region produces strong Pb and S signals (inset). Elements of Si, O, and Cu (from support grid) are also detected. From the EDS spectrum, an atomic ratio of 2.9:3.0 for Pb/S is calculated, which further confirms the formation of crystalline PbS nanoparticles inside the SBA-15. EDS provides a ratio of 2.9:35.6 for Pb:Si and 3.0:35.6 for S:Si, indicating 8% molar percent of PbS loading. Similar results were obtained with PbS nanowires. Figure 4c shows clearly that the nanowires are uniformly distributed within the channels of Ext-SBA-15. Furthermore, Figure 4d reveals that the average diameter is about 6 nm, which is consistent with the pore diameter of Ext-SBA-15. The lengths of the wires range from 50 to 200 nm. An EDS analysis shows that the nanowires consist of PbS crystal (an atomic ratio of 2.92:3.00 for Pb/S) and 18% molar percent of PbS loading.

Room-temperature PL spectra of PbS-SBA-15 samples are shown in Figure 5. With the excitation wavelength of 514.5 nm, the emission maximum of the PL spectra of PbS-particle-SBA-15 and PbS-wire-SBA-15 is around 665 nm and the corresponding energy gap is 1.87 eV. Compared with the bulk counterpart (0.41 eV), the nanosized PbS exhibits a massive blue shift in the PL spectrum, clearly indicating the quantum size effect.

The key for the transition from nanocrystals to nanowires is to increase the loading of inorganic compound in the meso-channels. The loading of PbS greatly depends on the amount of thiol functional groups that are obtained from the Si−OH groups on the surface of channels of SBA-15. Calcination at 550 °C for 6 h removes more Si−OH groups than does ethanol extraction, resulting in a decrease of reaction sites for the grafting of thiol groups. This has been confirmed by thermal gravimetric analysis (TGA) and UV−vis adsorption of Pb^{2+} solution. Compared with 4.5% weight loss of the SH-Cal-SBA-15 during 260∼330 °C, the SH-Ext-SBA-15 has a weight loss of 9.8%. The more weight loss in SH-Ext-SBA-15 means that more thiol groups have been introduced into the Ext-SBA-15. Another evidence to confirm that more thiol groups have been introduced into the channels of Ext-SBA-15 is from the UV−vis adsorption of Pb^{2+} solution (Figure 6). The same amount of Cal-SBA-15, SH-Cal-SBA-15, and SH-Ext-SBA-15 samples was loaded into a Pb^{2+} solution. For Cal-SBA-15, the absorbance at 270 nm is the same as the original Pb^{2+} solution (Figure 6a, b), while for SH-Cal-SBA-15 and SH-Ext-SBA-15, the absorbance decreases (Figure 6c and 6d), which demonstrates the adsorption of Pb^{2+} by the thiol groups. Furthermore, more Pb^{2+} have been absorbed into SH-Ext-SBA-15 than SH-Cal-SBA-15.

By adjusting the experimental conditions, the size and morphology of PbS nanocrystallites can be controlled. The

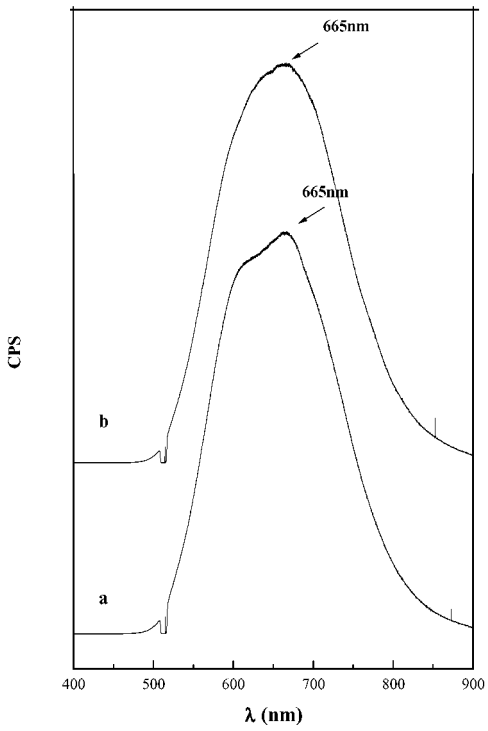

Figure 5. Photoluminescence spectra of (a) crystalline PbS nanoparticles and (b) crystalline PbS nanowires.

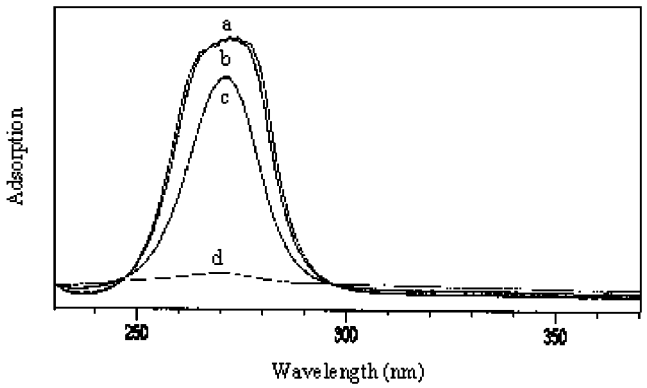

Figure 6. UV−vis adsorption spectra of (a) a Pb^{2+} solution; (b) after addition of Cal-SBA-15; (c) after addition of SH-Cal-SBA-15; (d) after addition of SH-Ext-SBA-15.

channel size of SBA-15 can be expanded up to 20 nm by the addition of a swelling agent of 1,3,5-trimethylbenene.[23] As a result, PbS nanocrystals and nanowires can be synthesized with controlled size. The synthesis of nanocrystals of 17.2 nm diameter has been achieved and verified with both TEM and XRD.

We have demonstrated a new synthetic procedure for the preparation of binary PbS nanocrystals and nanowires with a narrow size distribution by using mesoporous silica SBA-15 as a template. The thiol group surface modification technique allows separate introduction of $-S$ and Pb^{2+} in a nonreactive environment, leading to efficient loading of semiconductors into mesoporous materials. PbS nanocrystals with uniform sizes ($\sim$5 nm) are confirmed for the first time by high-resolution TEM to be inside the channels of mesoporous SBA-15. Binary PbS nanowires with uniform diameters ($\sim$6 nm) are prepared for first time by using mesoporous silica channels as the template. By changing the template removal process and by changing the mesoporous silica precursors, the size and morphology of the PbS nanocrystallites can be easily controlled.

Acknowledgment. The work was supported by National Natural Science Foundation of China (Grant 29873012 and 29925309), Education Ministry of China, Shanghai Technology Committee (00JC14014), Post-doctor Foundation, and by U. C. − Riverside.

References

(1) Colvin, V. L.; Schlamp, M. C.; Alivisatos, A. P. *Nature* **1994**, *370*, 354.
(2) Klein, D. L.; Roth, R.; Lim, A. K. L.; Alivisatos, A. P.; McEuen, P. L. *Nature* **1997**, *389*, 699.
(3) Ridley, B. A.; Nivi, B.; Jacobson, J. M. *Science* **1999**, *286*, 746.
(4) Alivisatos, A. P. *Science* **1996**, *271*, 933.
(5) Gallardo, S.; Gutierrez, M.; Henglein, A.; Janata, E.; *Ber Bunsen-Ges. Phys. Chem.* **1989**, *93*, 1080.
(6) Wang, Y. *Acc. Chem. Res.* **1991**, *24*, 133.
(7) Wang, Y.; Suna, A.; Mahler, W.; Kasowski, R. *J. Chem. Phys.* **1987**, *87*, 7315.
(8) Wang, S. Yang, S. *Langmuir* **2000**, *16*, 389.
(9) Wang, Y.; Herron, N. *J. Phys. Chem.* **1987**, *91*, 257.
(10) Kane, R. S.; Cohen, R. E.; Silbey, R. *Chem. Mater.* **1996**, *8*, 1919.
(11) Qiao, Z.; Xie, Y.; Xu, J.; Zhu, Y., Qian, Y. *J. Colloid Interface Sci.* **1999**, *214*, 459.
(12) Kresge, C. T.; Leonowicz, M. E.; Roth, W. J.; Vartuli, J. C.; Beck, J. S. *Nature* **1992**, *359*, 710.
(13) Parala, H.; Winkler, H.; Kolbe, M.; Wohlfart, A.; Fischer, R. A.; Schmechel, R.; Seggern, H. V. *Adv. Mater.* **2000**, *12*, 1050.
(14) Zhang W. H.; Shi J. L.; Wang L. Z.; Yan D. S. *Chem. Mater.* **2000**, *12*, 1408.
(15) Zhang W. H.; Shi J. L.; Chen H. R.; Hua Z. L.; Yan D. S. *Chem. Mater.* **2001**, *13*, 648.
(16) Chomski, E.; Dag, O.; Kuperman, A.; Coombs, N.; Ozin, G. A. *Chem. Vap. Deposition* **1996**, *2*, 8.
(17) Leon, R.; Margolese, D. I.; Stucky, G. D.; Petroff, P. M. *Phys. Rev. B* **1995**, *52*, R2285.
(18) Aronson, B. J.; Blanford, C. F.; Stein, A. *Chem. Mater.* **1997**, *9*, 2842.
(19) Srdanov, V. I.; Alxneit, I.; Stucky, G. D.; Reaves, C. M.; DenBaars, S. P. *J. Phys. Chem. B* **1998**, *102*, 3341.
(20) Agger, J. R.; Anderson, M. W.; Pemble, M. E.; Terasaki, O.; Nozue, Y. *J. Phys. Chem. B* **1998**, *102*, 3345.
(21) Hirai, T.; Okubo, H.; Komasawa, I. *J. Phys. Chem. B* **1999**, *103*, 4228.
(22) Winkler, H.; Birkner, A.; Hagen, V.; Wolf, I.; Schmechel, R.; von Seggern, H.; Fischer, R. A. *Adv. Mater.* **1999**, *11*, 1444.
(23) (a) Zhao, D.; Feng, J.; Huo, Q.; Melosh, N.; Fredrickson, G. H.; Chmelka, B. F.; Stucky, G. D. *Science* **1998**, *279*, 548. (b) Zhao, D.; Huo, Q.; Feng, J.; Chmelka, B. F.; Stucky, G. D. *J. Am. Chem. Soc.* **1998**, *120*, 6024.
(24) Han, Y. J.; Kim, J. M.; Stucky, G. D. *Chem. Mater.* **2000**, *12*, 2068.
(25) Huang, M. H.; Choudrey, A.; Yang, P. *Chem. Commun.* **2000**, 1063.
(26) Coleman, N. R. B.; O'Sullivan, N.; Ryan, K. M.; Crowley, T. A.; Morris, M. A.; Spalding, T. R.; Steytler, D. C.; Holmes, J. D. *J. Am. Chem. Soc.* 2001, in press.
(27) Fukuoka, A.; Sakamoto, Y.; Guan, S.; Inagaki, S.; Sugimoto, N.; Fukushima, Y.; Hirahara, K.; Iijima, S.; Ichikawa, M. *J. Am. Chem. Soc.* **2001,** *123*, 3373.
(28) Ryoo, R.; Kim, J. M.; Ko, C. H.; Shin, C. H. *J. Phys. Chem.* **1996**, *100*, 17718.
(29) Marler, B.; Oberhagemann, U.; Vortmann, S.; Gies, H. *Microporous Mater.* **1996**, *6*, 375.
(30) Sing, K. S. W.; Everett, D. H.; Haul, R. A.; Moscou, L.; Pierotti, R. A.; Rouquerol, J.; Sieieniewska, T. *Pure Appl. Chem.* **1985**, *57*, 603.
(31) Brunauer, S.; Emmett, P. H.; Teller, E. *J. Am. Chem. Soc.* **1938**, *60*, 309.
(32) Barrett, E. P.; Joyner, L. G.; Halenda, P. P. *J. Am. Chem. Soc.* **1951**, *73*, 373.

NL0156383